

# From capillary fracturing to blasting of wet granular materials

Dawang Zhang<sup>1,\*</sup> and Bjørnar Sandnes <sup>\*2</sup>

<sup>1</sup>College of Engineering, Swansea University, Crymlyn Burrows, Swansea, United Kingdom, SA1 8EN

<sup>\*</sup>College of Energy and Mining Engineering, Xi'an University of Science and Technology, Xi'an, 710049, China

November 20, 2025

## Abstract

Multiphase flows involving granular materials occur widely in nature and industry, yet still pose many research challenges because of the complexity of the mechanisms and interactions that govern their behaviour. Here we study experimentally the invasion of air by capillary fracturing into water-saturated granular packings confined in a Hele-Shaw cell. Small changes in packing density lead to the invasion pattern transitioning from capillary fracturing to pore invasion. By increasing the air pressure, the fractures widen and change from partially open to fully open. At the highest pressures studied here, a subsequent displacement of grains creates a cavity in the center region. In low-pressure experiments, increasing the plate spacing results in a transition from partially open to fully open fractures, while in higher-pressure experiments the subsequent displacement becomes less significant at larger plate spacing. Flow patterns with and without a semi-permeable outer boundary are compared, with the open boundary allowing grains to flow out of the cell, causing a widening of fractures as they approach the system edge.

## 1 Introduction

Multiphase granular flows are common in nature and engineering, and central to a wide range of processes including venting of methane from ocean sediments, migration of gasses in volcanic magma, and processing in food, pharmaceutical, chemical and geotechnical industries [1–13]. The injection of an invading fluid into a system containing granular materials submerged in a defending fluid has been shown to produce a large variety of flow patterns resulting from the combined effects of viscous, capillary, gravitational and frictional forces [14–27].

When a low-viscosity invading fluid displaces a high-viscosity defending fluid within a Hele-Shaw cell or porous media, the flow is viscously unstable at sufficiently high capillary number and viscosity ratio, resulting in viscous fingering (the Saffman-Taylor instability) [28–30]. When a granular material is present within the defending fluid, the meniscus between the two fluids can bulldoze the grains by capillary forces if the grains are wetted by the defending fluid (drainage). The bulldozing leads to the accumulation of a granular compaction front which is frictionally unstable, shaping the invading fluid into 'frictional fingers' or other patterns that plow the material

---

<sup>\*</sup>b.sandnes@swansea.ac.uk

to either side of the advancing front [31, 32]. When the filling level of granular material is relatively low, such that the material settles into a thin layer that is a fraction of the gap height, there is ample capacity for bulldozing and compacting of the bed. A large variety of flow patterns have been observed including frictional fingers [31, 33–35], bubbles [32, 36, 37], decompaction fingers [15, 38] and channeling [17, 39].

At high filling level (almost filling the entire gap), there is much less room for compacting of the bed. The invading fluid is observed to penetrate the packing in narrow and fracture-like branches. Chevalier *et al.* observed a transition from viscous fingering to fracturing in very dense suspensions of neutrally buoyant grains [40]. Jain and Juanes produced fracture formation in Discrete Element Model simulations and showed that the competition between capillary and frictional forces determined the transition from pore invasion (when the frictional strength of the material is greater than the maximum capillary stress limited by the pore invasion pressure) and fracturing (when capillary stress overcomes frictional strength) [16]. A phase diagram for the pattern formation was proposed in [32], while [41] coined the term ‘capillary fracturing’ and defined the ‘fracturing number’ as the dimensionless ratio between the mechanisms that promote fracturing (capillary and local viscous pressure gradients) and the frictional strength of the material. There are numerous other studies related to multiphase fracturing of granular beds (e.g. [1, 20, 21, 26, 42, 43]), and additional references can be found in the review by Juanes *et al.* [24].

Here we develop an experimental system to investigate capillary fracturing by air injection at high pressures up to 3 bar. We present the experimental results where we find that the fracturing patterns are sensitive to changes in injection pressure and volume fraction of the granular bed. We also discuss effects of plate spacing and boundary confinement on the pattern formation.

## 2 Methodology

A new Hele-Shaw setup and filling method was developed for this study. Because granular materials are prone to sedimentation, erosion, segregation and pattern formation, it can be challenging to achieve the uniform initial filling of the cell which is required for controlled experiments. Here we use a new strategy of injecting water through a grain-filled hopper such that the fluid-driven grain-flow eventually fills the cell. A semi-permeable outer boundary allows fluid to exit while containing the grains in the cell. The boundary is made of a strip of foam glued to the bottom plate in a circle with inner diameter 27.5 cm, centered on the inlet. Spacers with the thickness of 0.60, 0.75 and 0.90 mm in different experiments were put on the corners of the bottom plate. The two plates were then clamped together.

For the filling process, a large syringe (Labelled A in Fig. 1 a) is mounted directly above the inlet of the cell, connected by a short piece of tubing. This syringe is filled with water and a bed of sedimented grains, and acts as a silo/hopper for the filling. Through a hole in the top of syringe A, water is injected from another syringe B mounted on a syringe pump. The water flow, assisted by gravity, forces into the cell a dense mixture of water/grains, which spreads out in a circular shape until the grains come in contact with the foam boundary. Now a gradual compaction process follows, where the grain bed in the cell compactifies with continued injection. A certain control of the spatial uniformity and final filling fraction can be achieved by varying the imposed flow rate and the length of time the flow is maintained to compactify the packing, however the method has limitations in terms of the range of filling fractions that can be achieved, and problems with non-uniformity can still persist. After many trial-and-error studies, a flow rate of 10 ml/min was chosen to produce the most uniform beds, with the time (total injected volume) varied to produce different filling fractions within a limited range. The grains were glass beads sieved to a diameter range of 75 - 100  $\mu\text{m}$ . We can vary  $\phi$  by adjusting the filling parameters  $Q_{\text{fill}}$  and  $V_{\text{fill}}$ . In the following, the intermediate values of  $Q_{\text{fill}} = 10 \text{ mL/min}$  and  $V_{\text{fill}} = 48 \text{ mL}$

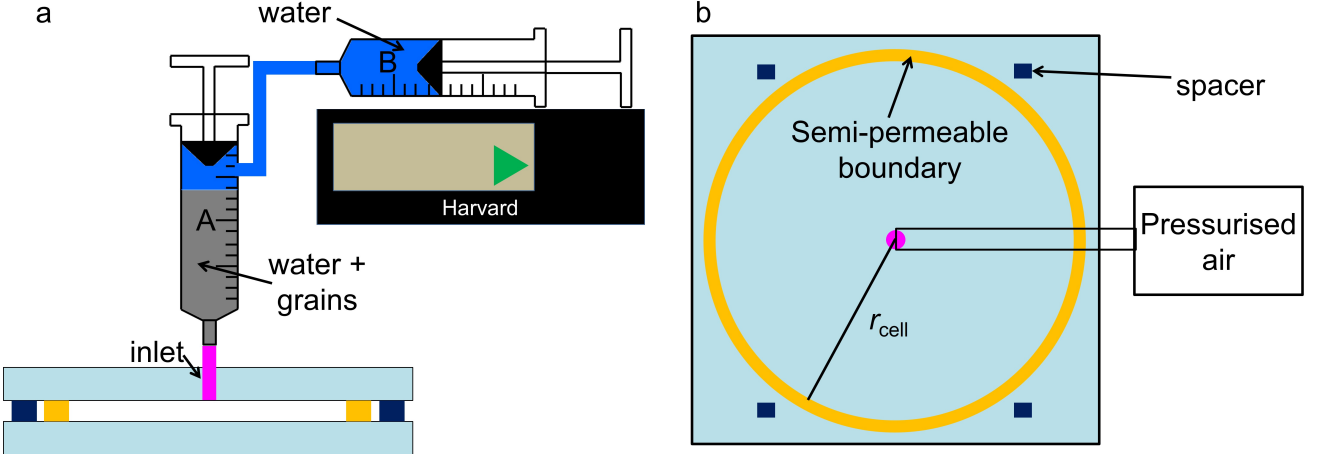


Figure 1: Illustration of the setup for fracturing experiments. (a) Preparation of granular packing. Water in syringe B was injected into syringe A thereby pushing a dense mixture of water and beads from syringe A into the cell. (b) Top view of the experimental setup. The inner radius of the granular packing confined by the semi-permeable boundary  $r_{\text{cell}} = 13.7 \pm 0.1$  cm. Pressurised air in a container is released into the cell by opening a valve.

were used, corresponding to a filling fraction  $\phi = 0.55$  which was observed to produce the most well-defined fracturing patterns.

After the filling procedure was completed, the silo syringe was removed, and the inlet was then connected up to a container with pressurised air. The container had been pressurised using an inflator (a bicycle pump). Air pressures used in this study ranged from 0.07 to 3 bar. Air pressure in the container was measured with a sensor (SensorTechnics) connected to a data acquisition system (compactDAQ, NI) and logged using LabView. The experiments commenced by rapid opening of a valve to let the pressurised air enter the cell at the central inlet.

The volume of the air container was approximately 1 L which is large compared to the internal volume of the cell ( $\approx 50 \text{ cm}^3$  at the largest gap size), with the volume displaced during the course of an experiment smaller still. We therefore make the assumption that the pressure decrease because of air expansion has negligible effect during an experiment. That is not to say that the pressure is everywhere equal to the reservoir pressure: there can be a significant pressure drop associated with the air flow through the very narrow fractures.

Initial experiments with different filling fractions reported in the next section were conducted using a syringe pump (PHD Ultra, Harvard Scientific) instead of the pressure reservoir. This allowed the fracturing process to be characterised at low pressure and constant injection rate similar to previous studies [21, 32], before moving on to experiments investigating higher pressures.

The cell was backlit using a white LED board. The experiment was filmed using a high-speed camera (Photron Fastcam 1024-PCI). The camera had a resolution of  $1024 \times 1024$  and a highest frame rate of 1000 fps. The longest experiment lasted for 2 min and the shortest experiment lasted for 0.06 s.

### 3 Results and discussion

#### 3.1 From capillary fracturing to capillary invasion

The filling process of the grain-water mixture affects the volume fraction of grains  $\phi$ , and hence the patterns formed. In the  $b = 0.6\text{mm}$  cell, an injected volume of  $V_{\text{fill}} = 44 \text{ mL}$  was just enough to fill the region inside the boundary and this resulted in a measured volume fraction of  $\phi = 0.53 \pm 0.01$ . Allowing the pumping to continue even after the mixture had reached the

edge caused ongoing compaction of the granular bed, with excess water exiting through the foam boundary.  $V_{\text{fill}} = 48 \text{ mL}$  produced a filling fraction  $\phi = 0.55 \pm 0.01$ , and  $V_{\text{fill}} = 52 \text{ mL}$  produced  $\phi = 0.58 \pm 0.01$ .  $\phi$  was obtained after the experiment: The mixture was collected and dried, the actual volume of the grains  $V_{\text{grain}}$  was calculated by measured mass over the density of the material. The total volume of the mixture is  $V_{\text{total}} = bA_{\text{cell}}$ , where  $A_{\text{cell}}$  is the area inside the boundary,  $b$  is the gap between the plates, and  $\phi$  was calculated as  $V_{\text{grain}}/V_{\text{total}}$ .

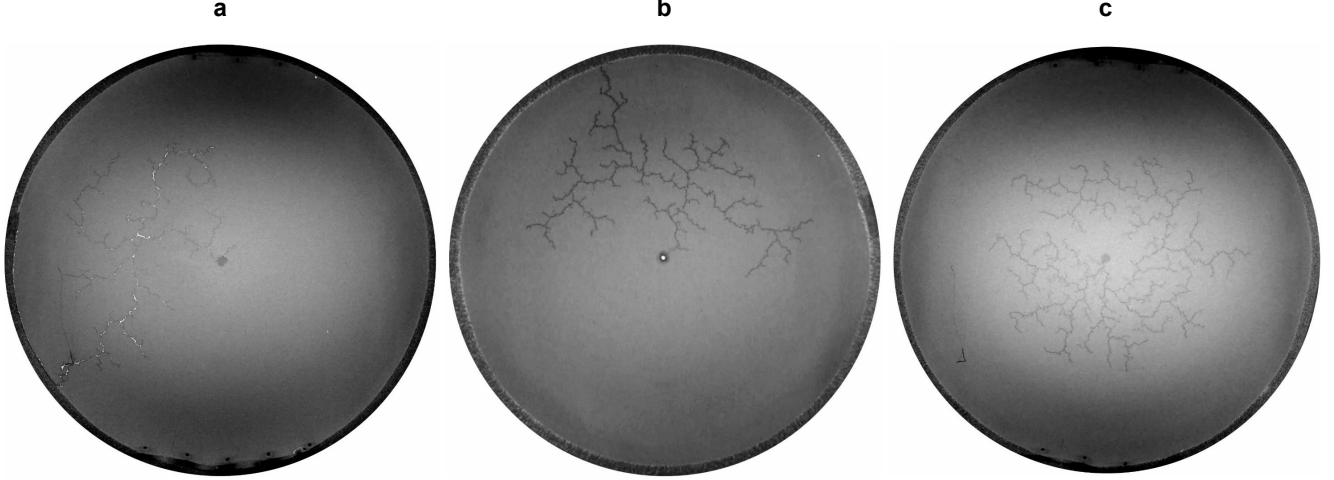


Figure 2: Fracturing patterns formed after air invading the grain-liquid packing with different volume fraction  $\phi$  (a) 0.53, (b) 0.55 (c) 0.58. In all panels, the diameter inside the boundary is 27.5 cm, injection rate is 0.01 mL/min.

Figure 2 shows the patterns formed after slow air injection into the granular packings with different  $\phi$  using the syringe pump with  $Q = 0.01 \text{ mL}/\text{min}$ , demonstrating that a small change in  $\phi$  can cause a drastically different pattern formation. At  $\phi = 0.53$  (2a), the fractures appear as white channels; the fractures are fully opened to enable the light from the panel above the cell to pass through to the camera placed underneath the cell. At  $\phi = 0.55$ , the fractures appear darker than the surrounding granular packing, the fractures are not fully opened and direct light is not able to pass unhindered through. the fractures appear dark in the backlit setting because of light scattering from the air-water-grain interfaces.

The experiment at the highest  $\phi = 0.58$ , a more complicated invasion is observed. We introduce  $t_n = t/t_{\text{all}}$  as a normalized time where  $t$  is the real time over the period of pattern formation and  $t_{\text{all}}$  is the whole time of pattern formation within the experiment system. The invasion started with partially opened, narrow fractures before  $t_n=2/10$ . The capillary pore invasion started later in the compacted area by early fracturing, with fracturing occurred simultaneously in the undisturbed area farther from the inlet. After  $t_n=3/10$ , the fracturing rarely occurred, capillary pore invasion dominated the pattern, the pore spaces of the granular packing were filled gradually.

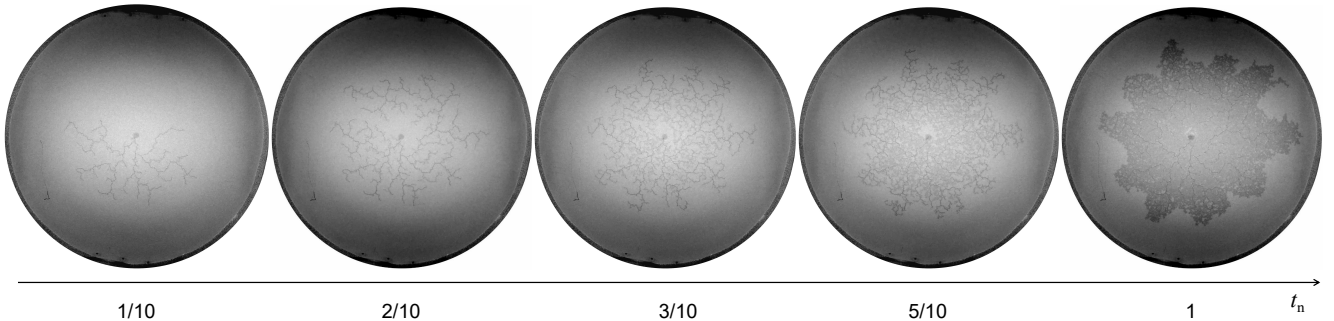


Figure 3: From fracturing to capillary pore invasion at  $\phi = 0.58$  at different time stages.

The experimental results with different  $\phi$  presented here all produce fractures, meaning that the

initial material is packed loose enough that the invading air/water meniscus is able to overcome local friction and deform the packing. Higher  $\phi$  constrains the amount of deformation, producing narrower fractures. At the highest  $\phi$ , the fracturing process has compacted all the material close to the inlet producing a higher frictional strength which exceeds the pore invasion pressure. Now it is easier to invade the pore space compared to deforming the hardened packing.

Holtzman et al. [41] achieved a transition from capillary fracturing to pore invasion by applying increasing confining weight on the water-grain packing. This transition is explained by the competition between the force provided by the invading air meniscus and the mechanical forces of the packing itself. Although we here present a different experimental situation, the principles behind the results may be similar. If the frictional forces exceeds the force provided by the air meniscus, then the capillary forces are not able to move the grains, and pore invasion occurs once the pore invasion threshold has been passed. In the opposite case, when the frictional strength is lower than the capillary pore invasion pressure, then the meniscus can deform the packing and open up fractures.

The monitored pressure in Fig. 4 indicates that the invading air pressure need to be built up to reach a fracturing pressure  $P_F$  after which the fracturing occurs and the pressure drops. Through this cyclic process (here naming as fracturing process) of pressure build-up, fracturing, and subsequent pressure drop, the fractures are able to propagate over time.

During capillary pore invasion process at  $\phi = 0.58$  after  $\approx 2000$  s in figure 4, the pressure keeps build up. This trend is consistent with two well-established mechanisms. Firstly, during primary drainage the average capillary pressure  $p_c(S_{def})$  increases as water saturation decreases, which raises the inlet pressure needed to continue invasion; this behavior is captured macroscopically by the Leverett  $J(S_w)$  framework and has been quantified jointly with relative permeability in core-flooding studies [44, 45].

$$J(S_{def}) = \frac{p_c(S_{def}) \sqrt{k_p/\eta}}{\gamma \cos \theta},$$

where  $k_p$  and  $\eta$  are permeability and porosity. The rise of  $\langle p_c \rangle$  with decreasing  $S_{def}$  thus elevates  $p_{in}$  as drainage progresses.

Secondly, the evolving two-phase invasion increases viscous pressure losses in both phases: the outer annulus available to the water phase narrows while the gas pathway lengthens, and the effective relative permeability change accordingly, producing a net rise in  $\Delta p_{visc}$ . Experiments and syntheses on air injection into water-saturated granular media support these dependencies on grain size and flow rate, and explain why steady or gradually rising inlet pressures are commonly observed [46, 47].

Although pore-scale imaging shows that Haines jumps generate transient pressure drops at individual throats [23, 48], several features of our setup (narrow throat-size distribution in bead packs, gas compressibility, and system compliance) can smooth high-frequency fluctuations, yielding a monotonic or weakly serrated pressure trace at the inlet.

In aspect of pressure evolution, the fracturing process is similar to Haines jumps [48, 49]. However the principles behind are different. The opening of fractures must overcome the fracturing pressure  $P_F$  which increases exponentially with  $L$  [21]:

$$P_F = P_T \exp \left( 2\mu\kappa \frac{L}{b} \right) \quad (1)$$

where  $P_T$  considers the effects of gravitational force, buoyancy and porosity  $n_0$ , can be written as:

$$P_T = \frac{1}{2} b \rho (1 - n_0) g = \frac{1}{2} b \rho \phi g \quad (2)$$

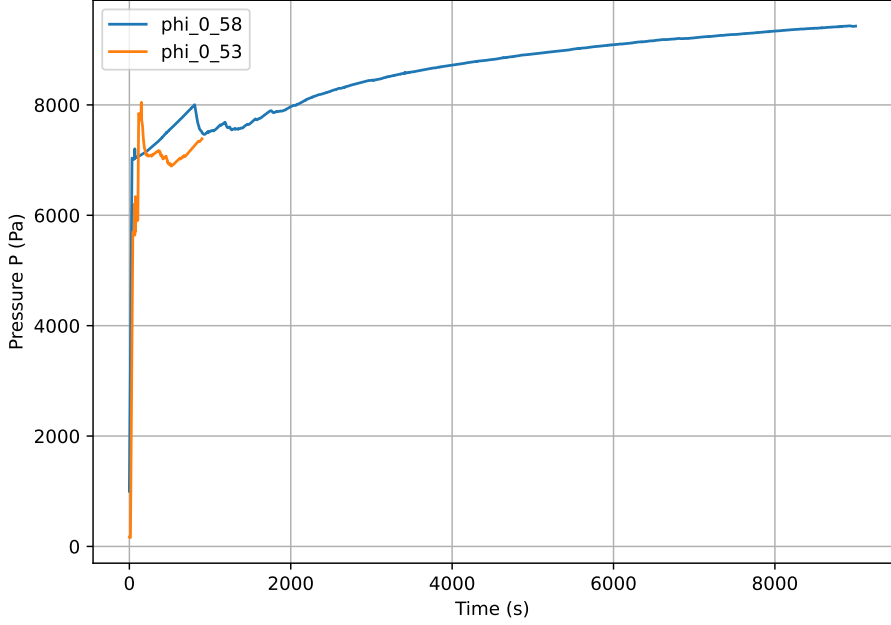


Figure 4: Pressure evolution with time by sensor in experiment. The pressure at fracture opening is around 8000 Pa for both  $\phi=0.53, 0.58$ .

The fracturing pressure  $P_F$  may naturally estimated by grain diameter  $d$  [21]. The maximum volume fraction of random close packing(RCP) is approximately  $\phi_{RCP} \approx 0.64$ , a result that has been confirmed by multiple experimental and theoretical studies [50, 51]. The granular packing in our system is not reaching RCP, thereby some free spaces are available for particles to move locally, which may means a smaller pressure for flow inside the granular material. We may reasonably assume that when the pore invasion occurs in Fig. 3 d where  $\phi=0.58$ , the granular packing is locally compacted to the RCP status, i.e.  $\phi = 0.64$ . We introduce a fraction coefficient to Laplace pressure equation[21], the fracturing pressure  $P_F$  may calculated by:

$$P_F = a \left(1 - \frac{\phi_{RCP}}{\phi}\right) \frac{4\gamma \cos \theta}{d} \quad (3)$$

Taking free variable  $a=2$ , contact angle  $\theta=12^\circ$ , the values of  $P_F$  calculated at different  $\phi$  0.53, 0.55, 0.58, 0.64 are 7290.26, 7565.36, 7978.012 and 8803.33 Pa separately, which are comparable to the experimental results in Fig. 4.

The frictional stress  $\sigma$  after the fracture is opened can be expressed as a function of the width of the front compaction  $L$ [32]:

$$\sigma = \frac{\rho g b}{2\kappa} \left[ (\kappa\mu + 1) \exp\left(\frac{2\mu\kappa L}{b}\right) - 1 \right] \quad (4)$$

where  $\rho = \phi(\rho_g - \rho_f)$ ,  $\rho_g$  the grain density,  $\rho_f$  the fluid density,  $\kappa$  Janssen's coefficient,  $\mu$  the friction coefficient,  $b$  the spacing gap.

The width of compaction front  $L$  can be estimated using Eq. 1. We use the following parameter values:  $\rho_f=1000$ ,  $\rho_g=2400$ ,  $\kappa=0.8$ ,  $\mu=0.53$ .  $\sigma$  is then calculated as 24480.96 Pa which is much lager than the pore enter pressure 8803.33 Pa, meaning a pore invasion is preferred and causing the invasion pattern transited from capillary fracture to capillary pore invasion.

### 3.2 From capillary fracturing to pneumatic caving

In the previous section, we investigated the invasion patterns of gas under quasi-static conditions. Upon further increasing the gas pressure, we observed more intriguing phenomena. We used

the pressurised air container and the high-speed camera in these cases. Figure 5 shows the patterns formed after air invasion at air pressures  $P_{\text{air}} = 0.07, 0.3, 1.0 and  $3.0$  bar. We observe three different invasion dynamics in these experiments: partially-opened fracturing, fully-opened fracturing, and fractures that keep widening over time. At  $P_{\text{air}} = 0.07$  bar, the fractures are darker than the surrounding granular packing, the fractures are not fully opened and the back-lighting is not able to penetrate the fractures. Higher pressure produces wider fractures, and fully opened fractures (thin white branches in the images) start to appear at  $P_{\text{air}} = 0.1$  bar.$

At  $P_{\text{air}} \geq 0.2$  bar, fully-opened fracturing dominates the invading process. In the mean time, we observe a gradual widening of the existing fractures with the invasion of air. This phenomenon becomes even more clear as we increase the initial air pressure. At  $P_{\text{air}} = 3$  bar, fractures initially propagate in a sweeping manner and followed by a "blast" forming an empty region close to the inlet.

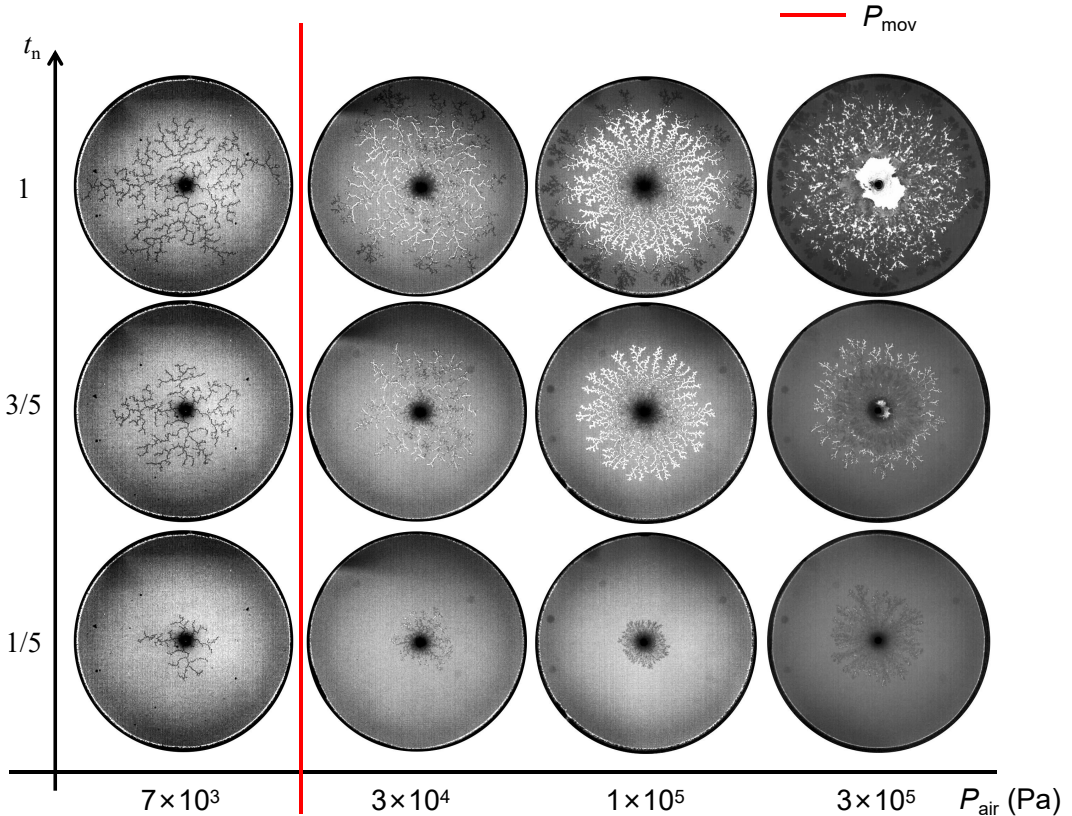


Figure 5: Patterns formed at different stages  $t_n$  after air invading to granular packing at air pressure  $P_{\text{air}}$  0.07 bar( $7 \times 10^3$  Pa), 0.3 bar( $3 \times 10^4$  Pa), 1 bar( $1 \times 10^5$  Pa) and 3 bar( $3 \times 10^5$  Pa).

To quantify the fractures here, we define several characteristic parameters after the first branch of the fractures reaches the boundary: normalized radius  $r_n = r_{\text{full}}/r_{\text{cell}}$  where  $r_{\text{full}}$  is the radius of fully-opened fracturing region and  $r_{\text{cell}}$  the inner radius of the boundary (shown in Figure 6), invaded area  $A_{\text{inv}}$ , all area within the boundary  $A_{\text{cell}}$ , fracture density  $A_{\text{inv}}/A_{\text{cell}}$ . We measure  $r_n$  and  $A_{\text{inv}}$ , and plot  $r_n$  and  $A_{\text{inv}}/A_{\text{cell}}$  as a function of air pressure as shown in Figure 6.

In Figure 6 b,  $r_n$  increases with the increase of the air pressure  $P_{\text{air}}$  when  $P_{\text{air}} \leq 0.2$  bar. Above 0.2 bar,  $r_n$  will keep at the same level. The fracture density  $A_{\text{inv}}/A_{\text{cell}}$  increases with the increase of  $P_{\text{air}}$ , which means that the air tends to invade more completely at a higher pressure.

We monitor the changes of grey level  $\Delta g_v$  of a selected region of interest (ROI) with time to characterise the gradual widening of fractures close to the inlet. The starting frame is chosen when the fractures within this region haven't become fully-opened. The grey level indicates the brightness of the image. We use a white LED board as back-light in the experiment, which results in the empty area in the packing appearing white in the image. Corresponding to the grey level of the monitored region, higher grey level means more fully-opened fractures.

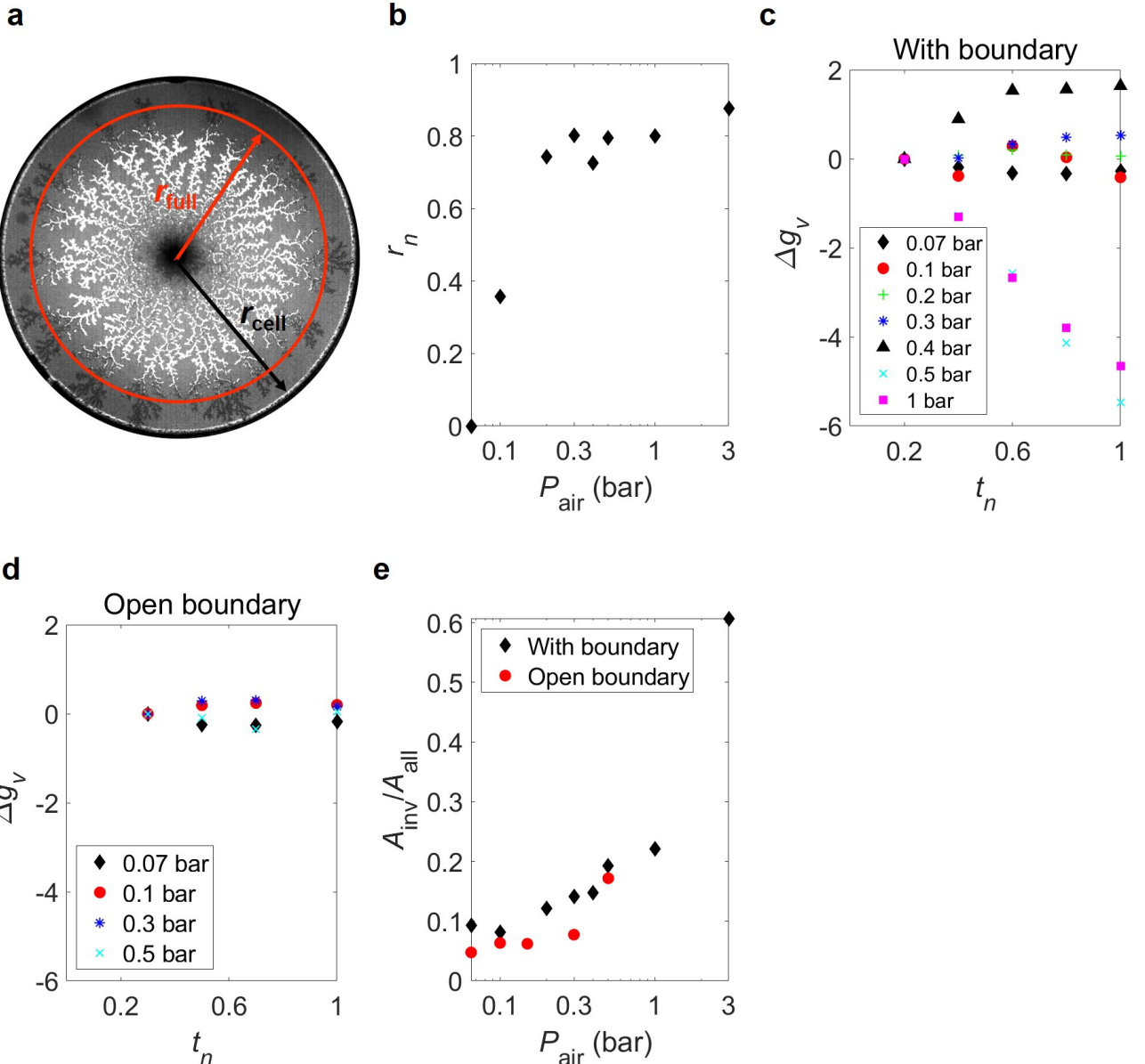


Figure 6: (a) Illustration of radius of fully-opened fracturing region  $r_{\text{full}}$  and radius of the granular packing  $r_{\text{cell}}$ . (b) Relationship between normalized number  $r_n = r_{\text{full}}/r_{\text{cell}}$ , and air pressure  $P_{\text{air}}$  in with-boundary experiments. X-axis is in log scale for better visualization. Grey level changes  $\Delta g_v$  at different stages  $t_n$  and different  $P_{\text{air}}$  of the with-boundary experiments (c) and the open-boundary experiments (d). (e) Relationship between fracture density  $A_{\text{inv}}/A_{\text{all}}$  and air pressure.

As seen in Figure 6 c,  $\Delta g_v$  shows a clear different trend at different  $P_{\text{air}}$ . The grey level remains more or less the same when  $P_{\text{air}} \leq 0.1$  bar and  $\Delta g_v$  remains approximately 0 throughout the experiment. This means there is no widening happening in already formed fractures.

At  $P_{\text{air}}$  0.3 and 0.4 bar, the grey level shows a clear increase with time, which means some of the fractures within the monitored region are widened and become fully opened with time. At  $P_{\text{air}}$  0.5 and 1 bar, the grey level in the ROI decreases with time. However, one can actually observe a widening of the fracture with time by eyes in Figure 5 e and f. This may be because there are more fractures branched in the center region with time. New fractures can cause a decrease of the grey level and if this decrease contributes more to the changes of grey level than the widening of the fracture, the overall grey level will decrease with time.

At the highest pressures studied here, we observe a clear darker ring (compaction zone) forming behind the fracture front (colored ring in Figure 8 a). This is caused by a displacement of the

material by the high pressure air after the initial fracturing. At  $P_{\text{air}}$  below 3 bar there are sometimes small-scale secondary displacements but not to a significant extent, and it has little effect on the patterns formed. At  $P_{\text{air}} \geq 3$  bar, this subsequent displacement becomes significant and causes the formation of a cavitation zone. The highly-compressed air blows the mixture of granular beads and water away from the center after the initial fracturing, caving the center area by the following air. The grey level decreases first and then increases dramatically.

Campbell *et al.* [21] studied the gas-driven fracturing at different injection rates  $Q$  and used the fracture density  $D$  to illustrate the patterns formed. They found a self-avoiding nature of the fracture network at low  $Q$  before the granular packing was fluidized. This self-avoiding phenomenon was caused by the resistance from the compaction front of the existing fracture. The width of the compaction front here was determined by the property of the packing itself, thereby almost the same fracture density was observed at different  $Q$  that could not fluidize the packing. After  $Q$  larger than the critical fluidization injection rate (0.2mL/min), the granular packing is fluidized and this resistance becomes smaller, causing an increase of  $D$  with  $Q$ . However, even at the maximum injection rate ( $Q = 100$  mL/min), the fracture patterns remained static once formed, and there was no reorganisation or subsequent deformation of the fractured zone in this previous study.

In the current study, we start the experiment at an air pressure 0.07 bar which is close to the peak pressure at  $Q = 100$  mL/min and similar experimental results are observed. At  $P_{\text{air}} > 0.1$  bar, we observe a new phenomenon — the elimination of existing fractures with air invasion. Figure 7 a shows the close-up images of fracture growth. Initially the “competition” between the fractures are small because there is enough space for them to grow. Later, new fractures nucleate behind, causing deformation of the already fractured material and the elimination of the existing fractures. Figure 7 b shows how a fracture ( $f_2$ ) is eliminated by another ( $f_1$ ).  $f_1$  moves towards  $f_2$  pushing forward the grain/liquid between them, fractures of  $f_2$  are gradually squeezed and finally closed.

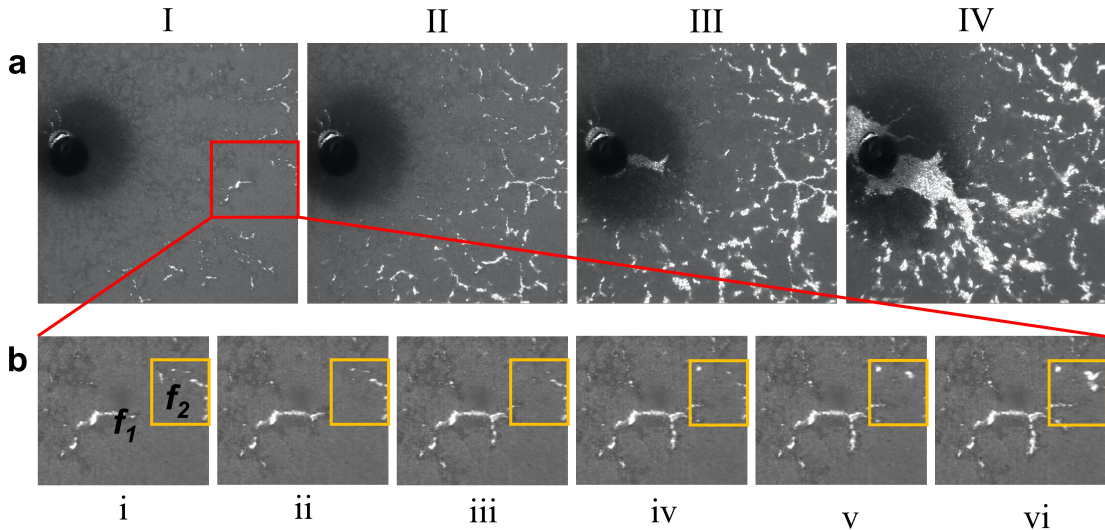


Figure 7: (a) Close-up images of air invasion at different time stages I–IV. (b) Processes i–vi of the elimination of the existing fracture.

At the beginning of blasting experiments at  $P_{\text{air}} \geq 1 \times 10^5 \text{ Pa}$ ,  $t_n = 1/5$  for instance, the invasion exhibits fast pore invasion, this may lead us the fact that the blasting of the granular packing by air may start from a Darcy-governed invasion, which builds up the pressure before structural failure of granular packing.

$$\mathbf{q}_w = -\frac{k}{\mu_w} \nabla p_w, \quad k \simeq \frac{\phi^3 d_p^2}{180(1-\phi)^2}. \quad (5)$$

where  $k$  is the permeability from Kozeny–Carman,  $d_p$  the particle diameter. This governs how pore pressure diffuses and builds up before any structural failure.

The pressure rapidly builds up in the cell and damages the structure formed by particle interactions. Using Eq. 4 in the last section, the calculated frictional stress of a compacted packing is the threshold pressure  $P_{\text{mov}}$  of beads moving. The theoretical value of 24480.96 Pa demonstrates good agreement with the experimental results. The invasion pattern exhibit capillary fracturing when the pressure is smaller than  $P_{\text{mov}}$ . Above this value, the invading air is able to push beads aside, and forming fully opened fractures as shown in Figure 5. At higher air pressure, the structure of granular packing is further damaged by fluidization, which causes fewer frictional stress thereby wider invasion channels and formation of the cavity.

### 3.3 Effect of plate spacing

We have also studied the effect of plate spacing  $b$  on pattern formation. Figure 8 shows the patterns formed by air invasion at different  $b$  and air pressure  $P_{\text{air}}$ . In Chapter 5, the effect of plate spacing on frictional fingers were studied, and it was found that larger  $b$  produced wider fingers because of the relative decrease in friction. Although the granular packing has been fluidized in all the experiments here and a fixed compaction front with certain width does not exist, differences in patterns formed at different  $b$  are clear to observe.

In Figure 8, At  $P_{\text{air}} = 0.07$  bar, the fractures are shown as partially opened in  $b = 0.60$  mm, and the fully-opened fractures start to occur in the center area in  $b = 0.75$  mm. At  $P_{\text{air}} = 1$  bar, fully-opened fractures occur in the central region in all the cases here. We also observe a clear decrease of  $r_n$  at larger  $b$  as shown in Figure 10 a.

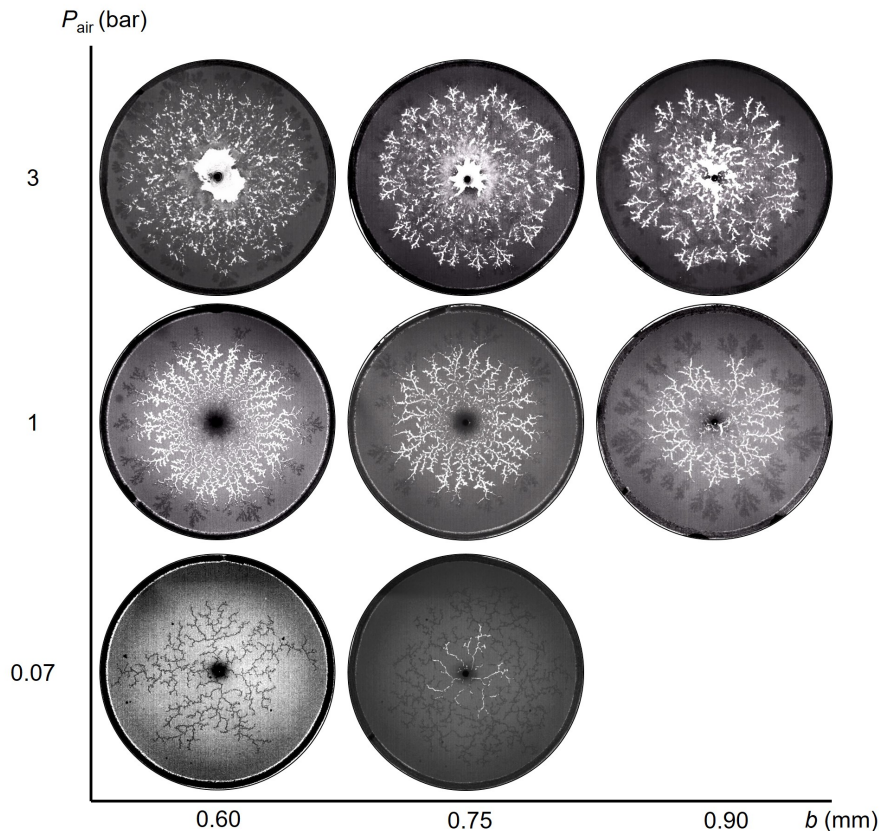


Figure 8: Air invasion patterns at different plate spacing  $b$  and air pressure  $P_{\text{air}}$ .

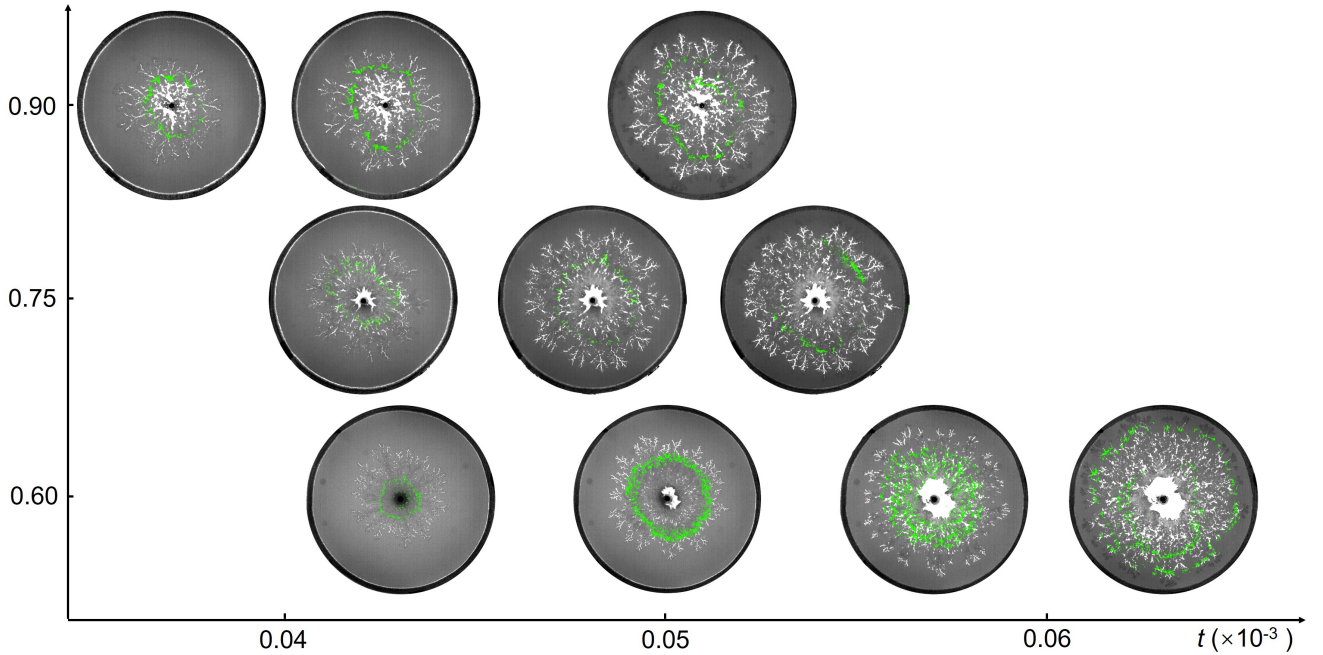


Figure 9: Time evolution of air invasion patterns at different plate spacing  $b$  at  $P_{\text{air}} = 3$  bar. Green rings in the figure highlights the compaction zone by pressurised air.

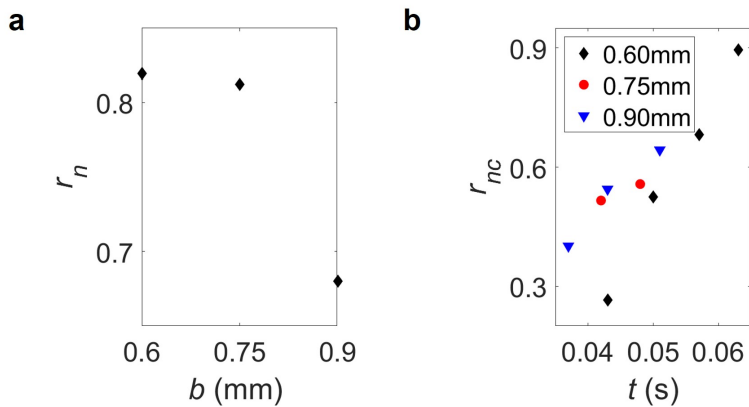


Figure 10: (a)  $r_n$  as a function of  $b$  and  $P_{\text{air}} = 1$  bar. (b) Time evolution of  $r_{nc}$  at different  $b$ .

At  $P_{\text{air}} = 3$  bar, the area of cavitation zone (white region in the pictures) in the packing center shows a clear decrease with the increase of  $b$ . The secondary displacement of granular materials by the air becomes significant on patterns formed only at  $P_{\text{air}} = 3$  bar, we subtract the pictures of invasion patterns at four stages before air breaks through the boundary and get the evolution of the compaction zones (green ring in Figure 9) caused by the secondary displacements. To quantify the scale of the secondary displacement, we define another normalized radius for the compaction zone  $r_{nc} = r_{\text{comp}}/r_{\text{cell}}$  where  $r_{\text{comp}}$  is the maximum radius of the compaction zone. The normalized radius  $r_{nc}$  increases with time at most of the cases. At higher  $b$ , the secondary displacement seems to occur earlier and the invading front reaches the boundary earlier. The compaction zone caused by the secondary displacement becomes smaller at higher  $b$ . One of the reason for these phenomena is the friction stress from the granular packing becomes smaller at higher  $b$ , and air is easier to move ahead than pushing the beads behind the invasion tips. In addition, larger  $b$  provides more spaces for the decompression of air, the pressure of the invasion air drops faster and becomes insufficient for large scale of secondary displacement. These experimental results are consistent with the relationship between  $b$  and  $\sigma$  in the theoretical formula Eq. 4.

### 3.4 Pattern formation after removing boundary

In the study above, the experiments were performed with the granular packing confined by a semi-permeable boundary. The following results were obtained with the boundary removed after the filling of the grain/liquid mixture was finished. Figure 11 shows the time evolution of air invasion at different air pressure. The main difference compared to the with-boundary experiments is that the fully-opened fractures occur in all cases and become wider in the region closer to the packing edge instead of in the center region. The partially-opened fractures are only observed in the center region of the packing and fewer at high-pressure experiments.

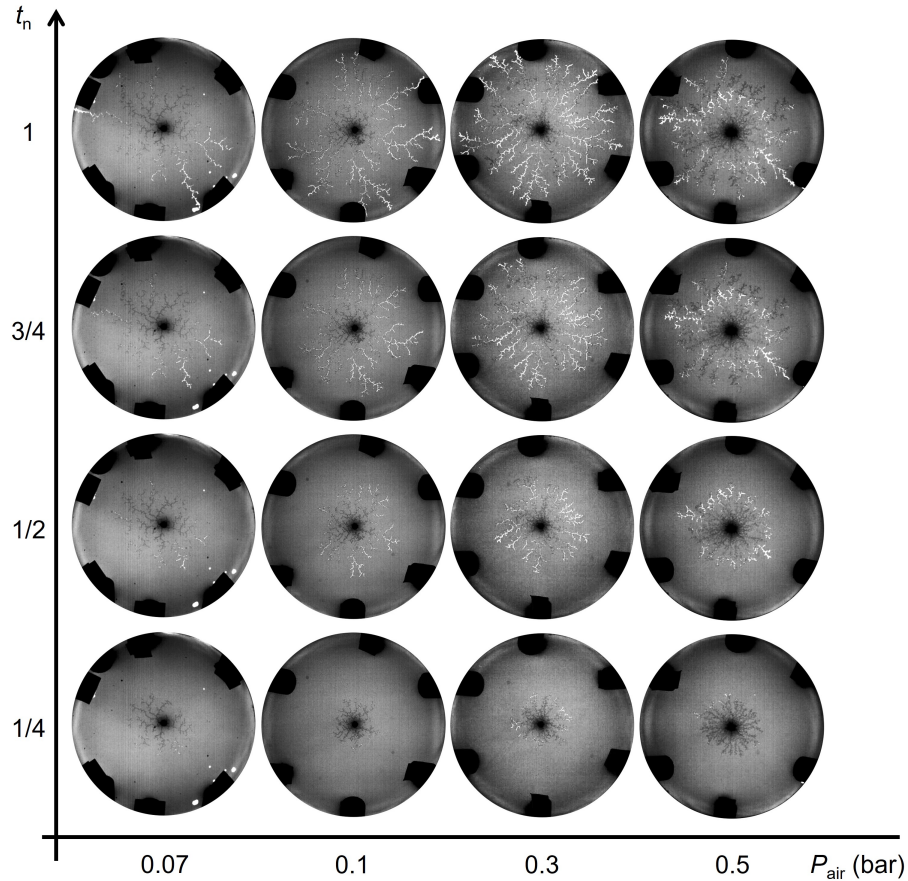


Figure 11: Time evolution of air invasion into the granular packing open boundary at different air pressure  $P_{\text{air}}$ .

With an open boundary, the grains are not held back at the perimeter of the cell, and the invading air set up a flow that pushes material outwards, leaving more space for widening of fractures. At  $P_{\text{air}} 0.07$  bar, there are partially-opened fractures occurring in the center region, but their branches expand in the region closer to the packing edge and become fully-opened (Figure 12 a), unlike the situation in with-boundary experiments (Figure 12 b). The region closer to the packing edge is easier to be fluidized than the inner region, because the force chains between the particles resist the fluidization of the packing and this resistance becomes much smaller in region close to the open edge. At higher pressure, the granular packing is fluidized further, thereby the fully-opened fractures are able to occur early in the center region.

Figure 12 shows the patterns formed in with- and open-boundary experiments at different  $P_{\text{air}}$ . Figure 6 c and d compare the grey level changes with time of the with- and open-boundary experiments at different pressure. The grey level almost has no change with time in with-out boundary experiments, which means there may be no widening of the fractures happened, while the grey level changes a lot in most of the cases of with-boundary experiments as has been described before. The process of the fracture widening is the process of pushing the compaction

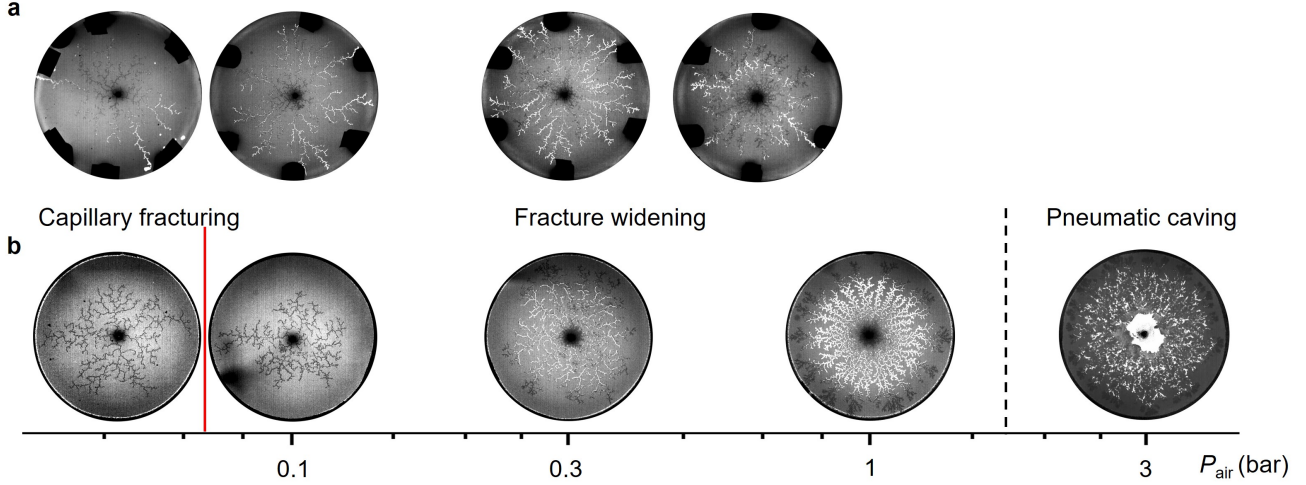


Figure 12: Pattern comparison in (a) open- and (b) with-boundary experiments at different air pressure. The red line in (b) distinguishes the capillary fracturing and the fracture widening, the black line distinguishes the pneumatic caving caused by a dramatic secondary displacement of the granular materials by the air. Figure a and b share the same axis of  $P_{\text{air}}$ .

front between the fractures further, which is much harder than pushing the looser region ahead of the invasion front, thereby the air choose to move forward instead of widening the fracture.

## 4 Conclusion

We have experimentally studied capillary fracturing of a water-saturated granular packing by pressurised air. The effects of filling fraction, pressure, boundary conditions and plate spacing are investigated. The capillary fracturing described in [41] is identified as partially-opened fracturing, and is achieved at the volume fraction  $\phi = 0.55$  in the current study. At slightly smaller  $\phi = 0.53$ , fully-opened fracturing is observed, and at slightly larger  $\phi = 0.58$ , capillary invasion after the fracturing is observed. The transition from capillary fracturing to capillary pore invasion is because the pore entry pressure is smaller than the frictional stress of the local compaction of granular beads. The experimental results of pattern transitions has a great agreement with the theoretical predication. We observe a clear darker ring (compaction zone) formed by the subsequent displacement of the air at higher pressure. The patterns formed at different pressures are different and can be divided into three phases: capillary fracturing, fracture widening, and pneumatic caving. Although the invading manner shows a dramatic "blasting" at high air pressure, the Darcy-governed invasion is needed for pressure build-up at early stage. In the experiments with larger plate spacing  $b$ , we observe a transition from partially-opened fracturing to fully-opened fracturing at lower pressure, and a reduction of the caving at higher pressure. The boundary also plays a significant role in pattern formation, more fully-opened fracturing is observed because the granular packing becomes easier to be fluidized in this case.

## Conflict of Interest Statement

The authors declare that the research was conducted in the absence of any commercial or financial relationships that could be construed as a potential conflict of interest.

## Acknowledgments

We thank Deren Ozturk for discussions. This research was funded by the Engineering and Physical Sciences Research Council [EP/S034587/1] (B.S., C.W.M.); the European Research Council (ERC) under the European Union’s Horizon 2020 Programme [Grant No. 805469] (C.W.M.); the China Scholarship Council (CSC) (D.Z.); and the Research Council of Norway through its Centres of Excellence funding scheme [262644] (E.G.F., K.J.M.).

## Data Availability Statement

The datasets [GENERATED/ANALYZED] for this study can be found in the [NAME OF REPOSITORY] [[LINK](#)].

## References

- [1] Benjamin P Scandella, Liam Pillsbury, Thomas Weber, Carolyn Ruppel, Harold F Hemond, and Ruben Juanes. Ephemerality of discrete methane vents in lake sediments. *Geophysical Research Letters*, 43(9):4374–4381, 2016.
- [2] Bernard P Boudreau, Chris Algar, Bruce D Johnson, Ian Croudace, Allen Reed, Yoko Furukawa, Kelley M Dorgan, Peter A Jumars, Abraham S Grader, and Bruce S Gardiner. Bubble growth and rise in soft sediments. *Geology*, 33(6):517–520, 2005.
- [3] Michael Riedel, Martin Scherwath, Miriam Römer, Mario Veloso, M Heesemann, and George D Spence. Distributed natural gas venting offshore along the Cascadia margin. *Nature Communications*, 9(1):1–14, 2018.
- [4] Xiaojing Fu, Joaquin Jimenez-Martinez, Thanh Phong Nguyen, J William Carey, Hari Viswanathan, Luis Cueto-Felgueroso, and Ruben Juanes. Crustal fingering facilitates free-gas methane migration through the hydrate stability zone. *Proceedings of the National Academy of Sciences*, 117(50):31660–31664, 2020.
- [5] Ning Li, Chuan Tang, Xianzheng Zhang, Ming Chang, Zhile Shu, and Xianghang Bu. Characteristics of the disastrous debris flow of chediguan gully in yinxing town, sichuan province, on august 20, 2019. *Scientific reports*, 11(1):1–18, 2021.
- [6] Andrea Parmigiani, Salah Faroughi, C Huber, Olivier Bachmann, and Y Su. Bubble accumulation and its role in the evolution of magma reservoirs in the upper crust. *Nature*, 532 (7600):492–495, 2016.
- [7] Katharine V Cashman, R Stephen J Sparks, and Jonathan D Blundy. Vertically extensive and unstable magmatic systems: a unified view of igneous processes. *Science*, 355(6331): eaag3055, 2017.
- [8] Sam Poppe, Johan T Gilchrist, Eric Christophe Pascal Breard, Alison Graettinger, and Stephen Pansino. Analog experiments in volcanology: towards multimethod, upscaled, and integrated models. *Bulletin of Volcanology*, 84(5):1–19, 2022.
- [9] J Oppenheimer, A Capponi, KV Cashman, SJ Lane, AC Rust, and MR James. Analogue experiments on the rise of large bubbles through a solids-rich suspension: A “weak plug” model for strombolian eruptions. *Earth and Planetary Science Letters*, 531:115931, 2020.

- [10] Anthony Philpotts and Jay Ague. *Principles of igneous and metamorphic petrology*. Cambridge University Press, 2009.
- [11] Jacques Duran. *Sands, powders, and grains: an introduction to the physics of granular materials*. Springer Science & Business Media, 2012.
- [12] Fernando J Muzzio, Troy Shinbrot, and Benjamin J Glasser. Powder technology in the pharmaceutical industry: the need to catch up fast, 2002.
- [13] Eric Dickinson. Food emulsions and foams: Stabilization by particles. *Current Opinion in Colloid & Interface Science*, 15(1-2):40–49, 2010.
- [14] Christophe Chevalier, A Lindner, and E Clément. Destabilization of a saffman-taylor finger-like pattern in a granular suspension. *Phys. Rev. Lett.*, 99(17):174501, 2007.
- [15] Xiang Cheng, Lei Xu, Aaron Patterson, Heinrich M Jaeger, and Sidney R Nagel. Towards the zero-surface-tension limit in granular fingering instability. *Nature Physics*, 4(3):234–237, 2008.
- [16] A. K. Jain and R. Juanes. Preferential mode of gas invasion in sediments: Grain-scale mechanistic model of coupled multiphase fluid flow and sediment mechanics. *Journal of Geophysical Research: Solid Earth*, 114(B8), 2009. doi: <https://doi.org/10.1029/2008JB006002>.
- [17] Germán Varas, Valérie Vidal, and Jean-Christophe Géminard. Venting dynamics of an immersed granular layer. *Physical Review E*, 83(1):011302, 2011.
- [18] Haiying Huang, Fengshou Zhang, Patrick Callahan, and Joseph Ayoub. Granular fingering in fluid injection into dense granular media in a hele-shaw cell. *Physical review letters*, 108(25):258001, 2012.
- [19] Fredrik K Eriksen, Renaud Toussaint, Knut J Måløy, and Eirik G Flekkøy. Invasion patterns during two-phase flow in deformable porous media. *Frontiers in Physics*, 3:81, 2015.
- [20] Julie Oppenheimer, Alison Rust, Katharine Cashman, and Bjørnar Sandnes. Gas migration regimes and outgassing in particle-rich suspensions. *Frontiers in Physics*, 3, 2015. doi: 10.3389/fphy.2015.00060.
- [21] James M Campbell, Deren Ozturk, and Bjørnar Sandnes. Gas-driven fracturing of saturated granular media. *Phys. Rev. Appl.*, 8(6):064029, 2017.
- [22] Marie-Julie Dalbe and Ruben Juanes. Morphodynamics of fluid-fluid displacement in three-dimensional deformable granular media. *Physical Review Applied*, 9(2):024028, 2018.
- [23] Zhonghao Sun and J. Carlos Santamarina. Grain-displacive gas migration in fine-grained sediments. *Journal of Geophysical Research: Solid Earth*, 124(3):2274–2285, 2019. doi: <https://doi.org/10.1029/2018JB016394>.
- [24] Ruben Juanes, Yue Meng, and Bauyrzhan K. Primkulov. Multiphase flow and granular mechanics. *Phys. Rev. Fluids*, 5:110516, Nov 2020. doi: 10.1103/PhysRevFluids.5.110516.
- [25] Kun Xue, Panpan Han, Kaiyuan Du, Yixiang Gan, Ziwei Wang, and Chunhua Bai. Morphodynamics of a dense particulate medium under radial explosion. *Soft matter*, 16(6):1498–1517, 2020.
- [26] Yue Meng, Bauyrzhan K Primkulov, Zhibing Yang, Chung Yee Kwok, and Ruben Juanes. Jamming transition and emergence of fracturing in wet granular media. *Physical Review Research*, 2(2):022012, 2020.

- [27] Sungyon Lee, Jeremy Lee, Robin Le Mestre, Feng Xu, and Christopher W. MacMinn. Migration, trapping, and venting of gas in a soft granular material. *Phys. Rev. Fluids*, 5:084307, 2020. doi: 10.1103/PhysRevFluids.5.084307.
- [28] Philip Geoffrey Saffman and Geoffrey Ingram Taylor. The penetration of a fluid into a porous medium or hele-shaw cell containing a more viscous liquid. *Proc. R. Soc. Lond. A*, 245(1242): 312–329, 1958.
- [29] R. Lenormand, E. Touboul, and C. Zarcone. Numerical models and experiments on immiscible displacements in porous media. *Journal of Fluid Mechanics*, 189:165–187, 1988.
- [30] Knut Jørgen Måløy, Liv Furuberg, Jens Feder, and Torstein Jøssang. Dynamics of slow drainage in porous media. *Physical review letters*, 68(14):2161, 1992.
- [31] B Sandnes, H A Knudsen, K J Måløy, and E G Flekkøy. Labyrinth patterns in confined granular-fluid systems. *Phys. Rev. Lett.*, 99(3):038001, 2007.
- [32] B Sandnes, E G Flekkøy, H A Knudsen, K J Måløy, and H See. Patterns and flow in frictional fluid dynamics. *Nature Comms.*, 2(1):1–8, 2011.
- [33] Henning Arendt Knudsen, Bjørnar Sandnes, Eirik Grude Flekkøy, and Knut Jørgen Måløy. Granular labyrinth structures in confined geometries. *Phys. Rev. E*, 77(2):021301, 2008.
- [34] Jon Alm Eriksen, Renaud Toussaint, Knut Jørgen Måløy, Eirik Flekkøy, and Bjørnar Sandnes. Numerical approach to frictional fingers. *Phys. Rev. E*, 92(3):032203, 2015.
- [35] Jon Alm Eriksen, Renaud Toussaint, Knut Jørgen Måløy, Eirik Flekkøy, Olivier Galland, and Bjørnar Sandnes. Pattern formation of frictional fingers in a gravitational potential. *Phys. Rev. Fluids*, 3(1):013801, 2018.
- [36] B. Sandnes, E.G. Flekkøy, and Måløy. Stick slip displacement of confined granular mixtures: Bubble expansion. *Eur. Phys. J. Spec. Top.*, 204:19–25, 2012.
- [37] Jon Alm Eriksen, Benjy Marks, Bjørnar Sandnes, and Renaud Toussaint. Bubbles breaking the wall: Two-dimensional stress and stability analysis. *Physical Review E*, 91(5):052204, 2015.
- [38] Fredrik K Eriksen, Renaud Toussaint, Antoine L Turquet, Knut J Måløy, and Eirik G Flekkøy. Pneumatic fractures in confined granular media. *Physical Review E*, 95(6):062901, 2017.
- [39] R. Poryles, G. Varas, and V. Vidal. Stability of gas channels in a dense suspension in the presence of obstacles. *Phys. Rev. E*, 95:062905, 2017.
- [40] C Chevalier, A Lindner, M Leroux, and E Clément. Morphodynamics during air injection into a confined granular suspension. *J. Non-Netwon. Fluid Mech.*, 158(1-3):63–72, 2009.
- [41] Ran Holtzman, Michael L Szulczewski, and Ruben Juanes. Capillary fracturing in granular media. *Physical review letters*, 108(26):264504, 2012.
- [42] Amina Islam, Sylvie Chevalier, Imen Ben Salem, Yves Bernabe, Ruben Juanes, and Mohamed Sassi. Characterization of the crossover from capillary invasion to viscous fingering to fracturing during drainage in a vertical 2d porous medium. *International journal of multiphase flow*, 58:279–291, 2014.

- [43] J. Suckale, T. Keller, K. V. Cashman, and P.-O. Persson. Flow-to-fracture transition in a volcanic mush plug may govern normal eruptions at stromboli. *Geophysical Research Letters*, 43(23):12,071–12,081, 2016.
- [44] M. C. Leverett. Capillary behavior in porous solids. *Transactions of the AIME*, 142(1): 152–169, 1941. doi: 10.2118/941152-G.
- [45] Ricardo Pini and Sally M. Benson. Simultaneous determination of capillary pressure and relative permeability curves from core-flooding experiments with various fluid pairs. *Water Resources Research*, 49(6):3516–3530, 2013. doi: 10.1002/wrcr.20274.
- [46] Idan Ben-Noah, Shmulik P. Friedman, and Brian Berkowitz. Air injection into water-saturated granular media—a dimensional meta-analysis. *Water Resources Research*, 58(9): e2022WR032125, 2022. doi: 10.1029/2022WR032125.
- [47] Idan Ben-Noah, Shmulik P. Friedman, and Brian Berkowitz. Dynamics of air flow in partially water-saturated porous media. *Reviews of Geophysics*, 61(2):e2022RG000798, 2023. doi: 10.1029/2022RG000798.
- [48] Steffen Berg, Holger Ott, Stephan A Klapp, Alex Schwing, Rob Neiteler, Niels Brussee, Axel Makurat, Leon Leu, Frieder Enzmann, Jens-Oliver Schwarz, et al. Real-time 3d imaging of haines jumps in porous media flow. *Proceedings of the National Academy of Sciences*, 110 (10):3755–3759, 2013.
- [49] Ryan T Armstrong and Steffen Berg. Interfacial velocities and capillary pressure gradients during haines jumps. *Physical Review E*, 88(4):043010, 2013.
- [50] J. D. Bernal. Random close-packed hard-sphere model. *Nature*, 185:68–70, 1960. doi: 10.1038/185068a0.
- [51] S. Torquato, T. M. Truskett, and P. G. Debenedetti. Is random close packing of spheres well defined? *Physical Review Letters*, 84(10):2064–2067, 2000. doi: 10.1103/PhysRevLett.84.2064.